Improved tree-ring sampling strategy enhances the detection of key meteorological drivers of rockfall activity

Robin Mainieri, Christophe Corona, Jérôme Lopez-Saez, Markus Stoffel, David Toe, Sylvain Dupire, Nicolas Eckert, Franck Bourrier

Improved tree-ring sampling strategy enhances the detection of key meteorological drivers of rockfall activity

Article *in* Catena · June 2021

DOI: 10.1016/j.catena.2021.105179

CITATION
1

READS
142

8 authors, including:

Robin Mainieri
Office National des Forêts
15 PUBLICATIONS **92** CITATIONS
SEE PROFILE

Christophe Corona
French National Centre for Scientific Research
180 PUBLICATIONS **2,765** CITATIONS
SEE PROFILE

Jérôme Lopez Saez
University of Geneva
60 PUBLICATIONS **1,018** CITATIONS
SEE PROFILE

Contents lists available at ScienceDirect

Catena

journal homepage: http://ees.elsevier.com

Improved tree-ring sampling strategy enhances the detection of key meteorological drivers of rockfall activity

R. Mainieri [a,c,*], C. Corona [b], J. Lopez-Saez [d,e], M. Stoffel [d,e,f], D. Toe [a], S. Dupire [a,g], N. Eckert [c], F. Bourrier [c]

[a] Univ. Grenoble Alpes, INRAE, UR LESSEM, 2 rue de la Papeterie-BP 76, F-38400 St-Martin-d'Héres, France
[b] GEOLAB, UMR6042 CNRS/ Université Blaise Pascal, Maison des sciences de l'Homme, 63057 Clermont-Ferrand Cedex 2, France
[c] Univ. Grenoble Alpes, INRAE, UR ETNA, 2 rue de la Papeterie-BP 76, F-38400 St-Martin-d'Héres, France
[d] Institute for Environmental Sciences - University of Geneva, 66 bd Carl Vogt, CH-1227 Carouge, Switzerland
[e] Dendrolab.ch, Department of Earth Sciences, University of Geneva, 13 rue des Maraîchers, CH-1205 Geneva, Switzerland
[f] Department F.A. Forel for Environmental and Aquatic Sciences, University of Geneva, 66 Boulevard Carl-Vogt, CH-1205 Geneva, Switzerland
[g] SylvaLab, FR-38530 Barraux, France

ARTICLE INFO

Keywords
Rockfalls
Dendrogeomorphology
Sampling strategy
Meteorological drivers of rockfall activity
Non-glaciated calcareous cliff
French Alps

ABSTRACT

To overcome the lack of historical archives at active rockfall environments, dendrogeomorphic techniques have been used extensively on forested slopes since the early 2000s and several approaches developed to extract rockfall signals from tree-ring records. Given the unpredictable nature of rockfall, these reconstructions are, in principle, of great help when it comes to relate fluctuations in rockfall activity to meteorological variables. Yet, so far, dendrogeomorphic time series were only rarely compared with meteorological records. Here, we ascribe this shortfall to the absence of clear guidelines on how to optimize the sampling strategy. In order to test this hypothesis, we capitalize on the extensive dataset of rockfall impacts recorded in trees growing in a mixed forest plot within the French Alps. We designed six different scenarios retrospectively and compared rockfall reconstructions with meteorological records. Our results demonstrate that reconstructions that include trees located in the most active segments of the plot (i.e. close to the cliff and over periods lacking multidecadal trends in the reconstruction) capture summer precipitation as the main driver of rockfall activity more clearly. This result is in line with monitoring studies from calcareous cliffs in the Alps located outside periglacial environments thus confirming the robustness of our approach.

1. Introduction

Rockfall is one of the most frequent geomorphic phenomena in mountain environments. Individual rockfall events typically involve the independent movement of individual rock fragments detaching from bedrock and propagating downslope bybouncing, falling or rolling down a slope (Selby, 1993). Rockfall can lead to significant economic losses and even casualties (Gardner, 1970; Erismann and Abele, 2001; Dussauge-Peisser, 2002; Hantz et al., 2003; Eckert et al., 2020). The unpredictable nature of rockfalls therefore often is of concern to authorities and decision makers (Corona et al., 2017). Hence, hazard quantification is critically needed, and should ideally be based on quantitative data providing information on the temporal probability of failure of rock masses expressed in terms of frequency or return period. The latter, often estimated using site-specific rockfall inventories, provides the mean number of events that occur within a given time period (Ferrari et al., 2016).

Yet, long-term records of rockfalls remain scarce and usually very fragmentary, especially in areas where risk associated with rockfall events rises proportionally with increasing urbanization (Favillier et al., 2015). To overcome this lack of historical archives, rockfall frequency and failure have been estimated in the past using sediment traps (Sass, 2005), terrestrial laser scans (Rabatel et al., 2008; D'Amato et al., 2016), or time-lapse cameras (Kellerer-Pirklbauer and Rieckh, 2016). Even though these methods allowed investigation of specific events (Matsuoka, 2019; Imaizumi et al., 2020), detailed rockfall monitoring efforts rarely exceed a few years at a specific site (Weber et al., 2019) and thus fail to encompass the typically wide range of rockfall processes on a slope (Sass, 2005). On forested slopes, tree damage and its dating with dendrogeomorphic approaches have been used widely to reconstruct past process activity (Stoffel and Corona, 2014). A review of these studies was conducted by Mainieri et al. (2019a) to include 25 rockfall reconstructions employing dendrogeomorphic approaches.

* Corresponding author at: Univ. Grenoble Alpes, INRAE, UR LESSEM, 2 rue de la Papeterie-BP 76, F-38400 St-Martin-d'Héres, France.
E-mail address: robin.mainieri@inrae.fr (R. Mainieri)

https://doi.org/10.1016/j.catena.2021.105179
Received 23 July 2020; Received in revised form 8 December 2020; Accepted 12 January 2021
Available online xxx
0341-8162/

Paradoxically, whereas tree-ring series have been used extensively to quantify rockfall frequency variations over time, dendrogeomorphic studies have only rarely attempted – with the exception of Perret et al. (2006), Šilhán et al. (2011), Zielonka and Wronska-Walach (2019) and Mainieri et al. (2020) – to identify drivers or to correlate changes in rockfall frequency with changing weather conditions. This scarcity of analyses on rockfall drivers is explained partly by the absence of clear guidelines regarding the sampling strategy required to obtain reliable chronologies that can be used for comparison with meteorological time series. Perret et al. (2006) demonstrated that the use of a systematic sampling– i.e. the coring of trees along linear transects with equal distances between each sampled tree irrespective of the presence of visible scars on its trunk– provides adequate data to derive a reconstruction of past rockfall events. Similarly, Morel et al. (2015) and Trappmann and Stoffel (2015) recommended a minimum sample size of 40–80 trees/ha to obtain rockfall chronologies of reasonable quality. By contrast, Gsteiger (1993) called for a homogeneous distribution of trees within the upper portions of the slope. None of the above studies has, however, investigated the influence of different sampling strategies on the detection of meteorological drivers so far.

In a majority of studies, the almost systematic, increasing trend of rockfall activity over time has hampered comparison of reconstructions with meteorological time series and therefore also prevented precise detection of drivers of rockfall (Trappmann et al., 2013). These non-climatic trends, related to the increasing number of growth disturbances (GDs) detected in tree-ring series over time, have been ascribed mainly to (1) the increase in sample depth and the increasing diameter that a tree exposes to rockfall with increasing age (Stoffel et al., 2005), (2) the difficulty of retrieving old, completely overhealed injuries (Stoffel and Perret, 2006; Trappmann and Stoffel, 2015) or (3) changing sensitivity of trees to record impacts with increasing age (Šilhán et al., 2013) or species (Trappmann et al., 2013; Favillier et al., 2015). Efforts have therefore been undertaken over the last decades to detrend rockfall reconstructions, that is to remove artificial increases in activity as one approaches the most recent past. Stoffel et al. (2005) therefore introduced a "rockfall rate" (RR) which takes the reduction of sample size and the decreasing exposed tree diameter (i.e. the decrease of 'target sizes' with smaller tree age) into account as one goes back in time. The approach, however, remains sensitive to artefacts related to (1) very small sample sizes at the beginning of the reconstructions and to (2) the increase of exposed diameters (Trappmann and Stoffel, 2015). More recently, Trappmann et al. (2014) and Trappmann and Stoffel (2015) revisited the RR to propose the use of a "Conditional Impact Probability" (CIP) where the authors quantified uncertainties related to potentially missed events in dendrogeomorphic rockfall reconstructions. Yet, CIP time series have not been used so far to detect potential meteorological drivers of and/or past fluctuations in past rockfall activity.

On this basis, this paper aims at determining the impacts of sampling strategies on the possibility to identify meteorological drivers of past rockfall events. Based on an unusually large dataset of rockfalls retrieved from growth disturbances (GD) in trees growing in a mixed forest plot in the French Alps (Mainieri et al., 2019a), we (1) built chronologies with different subsets of trees and different sampling procedures, (2) explore effects of sampling strategies on the reliability of reconstructed rockfall chronologies and finally (3) attempt to define and detect meteorological drivers of past rockfall events.

2. Study site

The study area is located on the territory of Saint-Guillaume (256 inhabitants), on the northern slope of the Pale mountain, close to the "Rocher du Bouchet", France (44°56′18″N, 5°35′11″E, 1350–1490 m asl, Fig. 1a). At the site, rockfall fragments are released from a 90-m-high, north-east-facing cliff (1450–1540 m asl, Fig. 1b) consisting of subhorizontally bedded Jurassic limestone (Tithonian) with narrow orthogonal joints. This structure favors the release of rock fragments with volumes not exceeding a few m^3. In the transit area (1380–1490 m asl), Quaternary scree is characterized by a convex-concave slope profile (26–46°, average: 38°) and a marked longitudinal sorting of debris with volumes of a few dm^3 at the apex to a few m^3 in the lower portion of the slope. The slope is covered by a mixed forest stand; at its bottom of the slope (1100 m asl), the slope is limited by a topographic berm (10°). In this study, we analyzed a tree plot of about 1 ha (110 × 90 m) located at the foot of the cliff (Fig. 1c) covered by a 800 trees ha^{-1} forest stand dominated by *Abies alba* (Silver fir), *Picea abies* (Norway spruce), *Acer pseudoplatanus* (Sycamore maple), *Fagus sylvatica* (Common beech), *Fraxinus excelsior* (European ash), *Sorbus aria* (White beam), *Sorbus aucuparia* (Mountain ash) and *Ulmus glabra* (Elm). Even though evidence of past logging (stumps) could not be found at the site, we cannot rule out the possibility that some limited silvicutural interventions did occur over the course of the last century. According to meteorological re-analyses data provided by SAFRAN (Durand et al., 2009), mean annual rainfall (1958–2017) is 951 mm and annual temperature averages 5.7 °C at the site. Rockfall is the predominant cause of damage observed on tree stems (Fig. 1e). However, in the uppermost portions of the talus slope, snow avalanches of limited extent are likely to occur as well. To limit uncertainties in the reconstruction, we only included scars that could undoubtedly be ascribed to rockfall and therefore also excluded growth suppression as it can potentially be caused by stem breakage following snow avalanche events.

No data on past geomorphic events exists in the municipal records. Yet, according to high-resolution maps computed for the study plot regarding (1) tree species, (2) tree age and (3) rockfall activity derived from a scar counting approach (Mainieri et al., 2019a; Mainieri et al., 2019b), a downslope decrease in the number of scars can be observed on individual stems. This finding is consistent with the well-known frequency reduction of fallen blocks as one moves down the slope (Gsteiger, 1989; Dorren et al., 2005; Dorren et al., 2006; Dorren et al., 2007). In addition, a clear difference is observed between the northwestern (where conifer trees dominate and where rockfall is more active) and the eastern (dominated by broadleaved species and with less rockfall active) compartments of the plot. The maps in Fig. 1 have been used to (1) design different sampling strategies, (2) select sampled trees (by avoiding trees that are located along the same trajectory) from the extensive dataset published by Mainieri et al. (2019a) (hereafter referred to as dat2019) and to (3) precisely assess the evolution of the CIP (see below).

3. Methods

3.1. Defining sampling strategies

dat2019 contains information retrieved from 1097 increment cores that have been sampled to date 603 scars in trees (372 on conifer and 231 on broadleaved trees) on 278 impacted stems. Using this dataset, we designed five different scenarios retrospectively representing different sampling strategies (S1-S5) (Fig. 2). For each tree extracted in scenarios S1-S5, we took an increment core (max. 40×0.5 cm) as close as possible to each visible scar, at the contact between the wound and the overgrowing callus tissue (Sachs, 2005; Larson, 1994; Schneuwly et al., 2009). In addition, based on the distribution of observed scars (which usually does not exceed 2 m in height), increments cores were systematically extracted from trees, in the fall line of rocks, at heights of 0.5, 1.0, and 1.5 meter, so as to maximize the probability to retrieve old masked injuries (Trappmann et al., 2014).

In the first scenario (S1), 161 trees including 101 conifers (*Abies alba, Picea abies*) and 60 broadleaved trees (*Fagus sylvatica, Sorbus aria, Acer pseudoplatanus*) with ages ranging from 97 to 96 years were randomly sampled from dat2019 over the 1.04 ha of the study plot, just by making sure that the selection of trees was random, yet representative of the relative abundance of tree species and diameter distributions observed at the plot (Fig. 2). In S2, trees were selected from dat2019

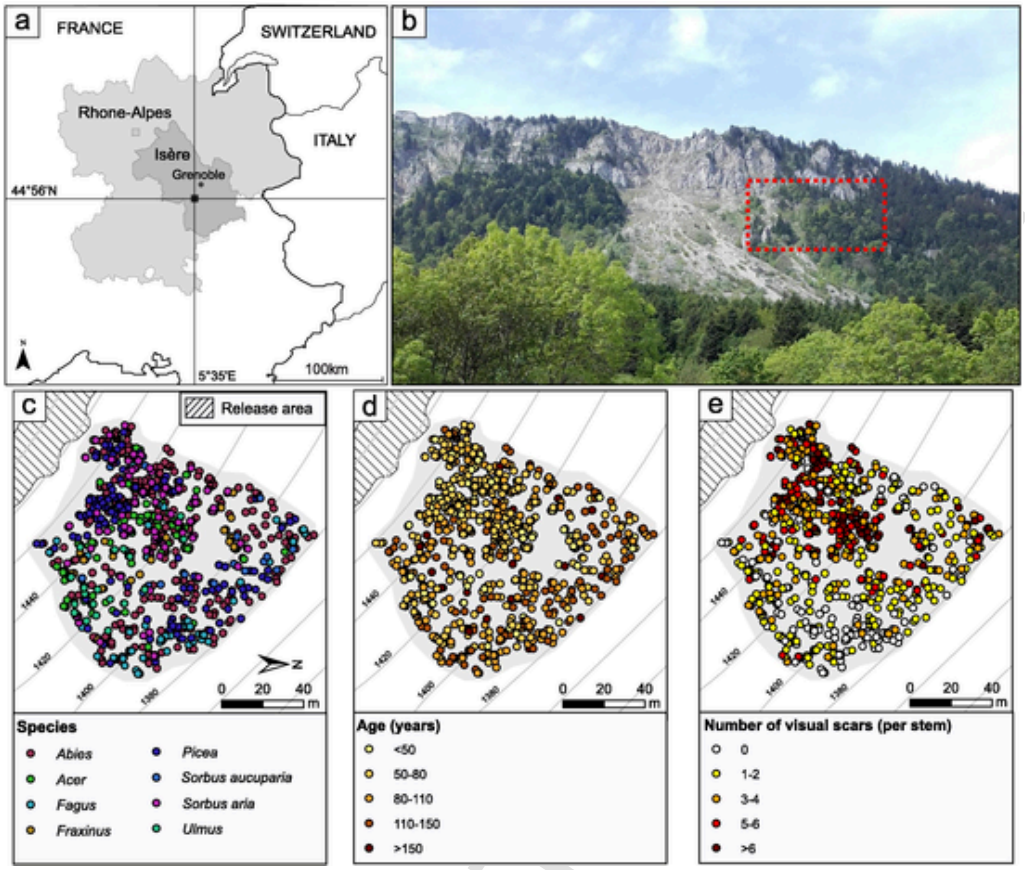

Fig. 1. The Rocher du Bouchet (a, b) slope is located in the Vercors massif (French Alps), Saint-Guillaume municipality. At the study plot, we identified (c) tree species, (d) tree age and (e) the number of scars visible on each individual stem. All information has been mapped at a 1-m resolution (Mainieri et al., 2019a).

with the idea to maximize the CIP, i.e. to intercept a maximum of potential rockfall trajectories while avoiding sampling several trees along the same trajectory. Scenarios S3-S5 are subsets of S2 for different compartments of the plot, namely the northern (S3), upper northern (S4), and southern compartments (S5). The spatial extent covered by each compartment was defined on the basis of visible wounds. The comparison between S3 – S5 is intended to show potential differences in meteorological drivers between the more active northern compartment of the plot – where the forest stand is dominated by conifers – and the southern compartment, where broadleaved trees show significantly smaller numbers of visible injuries. Scenarios S3-S4 have been designed to highlight potential effects of the increasing distance of trees from the cliff on both the rockfall chronology and the detection of meteorological drivers of process fluctuations. In scenario S6, additional sampling was carried out: a total of 127 cross-sections was cut from 24 stems in the upper northern part of the plot. Cross-sections were sawn at the level of each visible scar as well as systematically each 50 cm. All trees selected for destructive sampling had diameters at breast height (or DBH) <15 cm. More particularly, S6 aimed at investigating whether a restricted number of cross-sections, for which overhealed scars can still be found and the blurring of injuries is not a limiting factor, should be preferred over increment cores typically based on much more exhaustive sampling.

3.2. Dendrogeomorphic analyses

We prepared and analyzed samples following standard dendrochronological procedures proposed by Bräker (2002). In the laboratory, we measured tree rings (accuracy of 0.01 mm) using a digital LINTAB positioning table connected to a Leica stereomicroscope. For this investigation, we used the position of the first layer of callus tissue within the tree ring for intra-annual dating of rockfall damage. For *Abies alba* (Silver fir) and *Picea abies* (Norway spruce), traumatic resin ducts (TRDs) (Bannan, 1936; Stoffel, 2008; Stoffel and Bollschweiler, 2008) formed next to injuries (Schneuwly and Stoffel, 2008a; Schneuwly and Stoffel, 2008b) were used as an additional disturbance to date past rockfall events. The latter were only considered the result of rockfall activity if they formed compact and continuous tangential rows (Stoffel et al., 2005). Following Stoffel et al. (2005); Stoffel et al., 2005, the (i) presence of callus tissue and TRD next to (blurred) injuries, (ii) eccentric growth and the formation of reaction wood following stem tilting as well as (iii) abrupt growth releases were used as complementary lines of evidence for the dating of past rockfall damages. By contrast, growth suppression (GS) was excluded as it is more frequently caused by climate extremes (e.g. cold summers or drought), affecting radial growth for several years, than by rockfall events (Mainieri et al., 2020). Therefore, as GS could potentially increase noise in our reconstructions, they have been disregarded from analyses.

We applied the non-parametric Mann–Kendall (MK) test (Helsel and Hirsch, 1992) to detect potential trends in the reconstructed rockfall time series. This rank-based procedure was chosen as (1) it is suitable for non-normally distributed data, robust against (2) outliers and (3) data gaps. The MK test yields a trend test statistic allowing rejection of the null hypothesis at a certain significance level (Birsan et al., 2005). The slope of trends significant at the 95% level of the MK-test was estimated using the Theil-Sen method, which is suitable for nearly linear trends and has been shown to be mostly unaffected by non-normal data and outliers (Helsel and Hirsch, 1992). For each scenario, the MK test was computed over the 1959–2017 period covered by meteorological series, for moving time windows with lengths varying from 30 to 59 years.

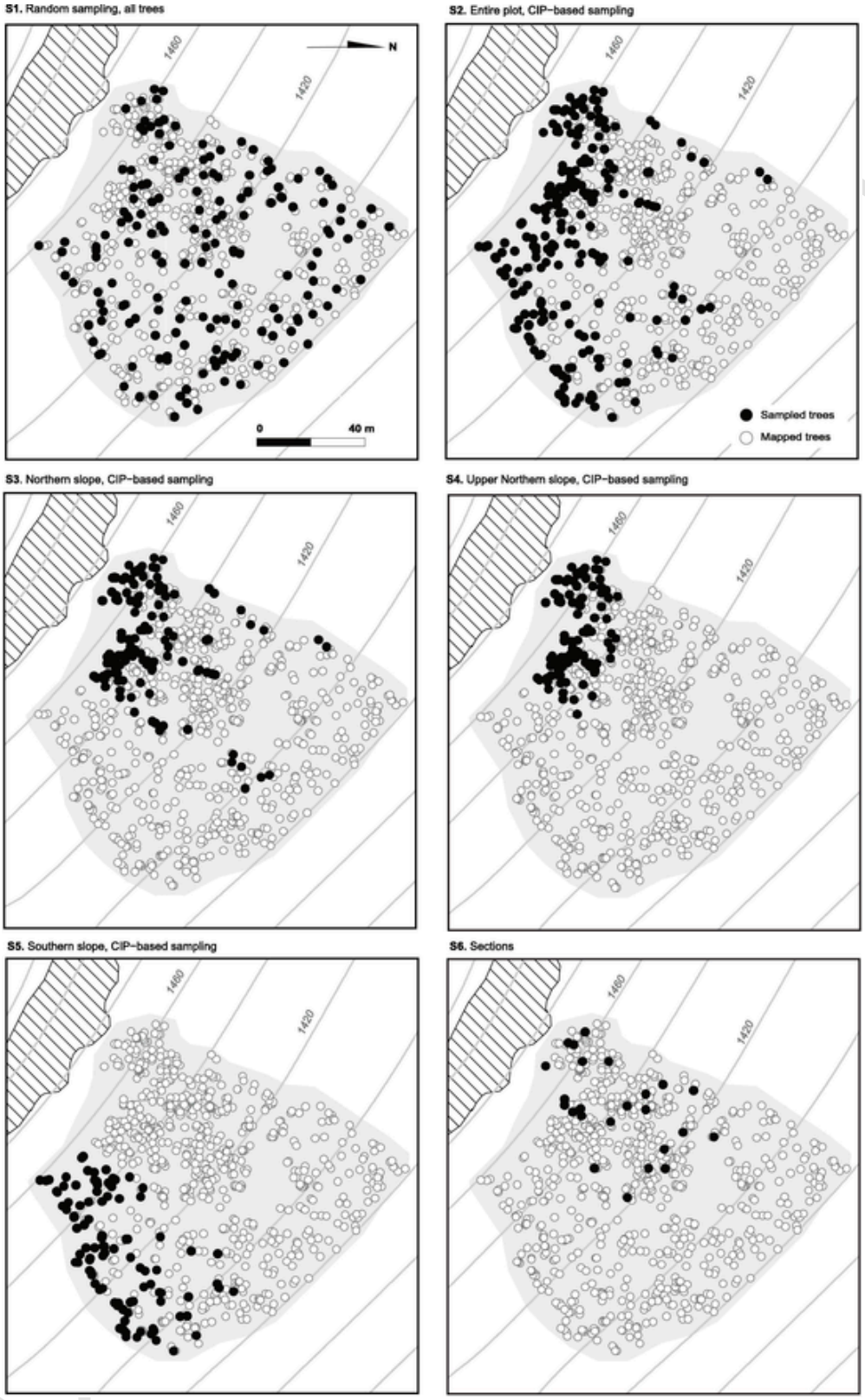

Fig. 2. Overview of the sampling strategy scenarios S1-S6. White circles represent all trees mapped in the forest plot, black circles represent the trees sampled in each of the scenarios.

3.3. Computation of the conditional impact probability

The conditional impact probability (CIP) approach, initially introduced by Moya et al. (2010), has been refined by Trappmann et al. (2013) and Favillier et al. (2017). It aims at quantifying the range covered by trees during a given year and has been used here to estimate the probability that blocks fall downslope without impacting any tree. The calculation of the CIP requires tree diameters and locations as well as an estimation of the mean diameter of falling blocks. The CIP concept is based on the idea that each tree is surrounded by a "circle of impact" which covers a range of the slope exposed to rockfall thereby defining a probability of a tree being impacted by a rock. This "circle of impact" represents a circular area centered on the tree stem and obviously depend on the tree's diameter at breast height (DBH) and the diameter of the rock (Ø). The range covered by trees in a given stand can therefore be computed as the sum of the impact circles (L_{IC}, Fig. 3 A B). Accordingly, with a given mean rock diameter, a known tree position and the DBH measured for of all trees, the CIP can be calculated for a plot as follows:

$$CIP = L_{IC}/L_{plot} \quad (1)$$

where L_{IC} is the cumulative length of the projections of "circles of impact" at the bottom of a plot, and L_{plot} is the length of the plot (i.e. 110 m in our case). Usually, the CIP is used to estimate the number of annually missed events and to quantify the quality and reliability of the reconstruction (Trappmann et al., 2013; Favillier et al., 2017). Here, in order to quantify precisely the evolution of the CIP back in time, polynomial diameter-age regressions have been used for each tree species (Mainieri et al., 2019a) to estimate the diameters of each tree within the plot and annually-resolved series of CIP. These series were then used to estimate real annual numbers of rockfalls (RR) as follows:

$$RR_t = NGD_t/CIP_t \quad (2)$$

where NGD_t represents the number of growth disturbances dated to year t and where CIP_t is the conditional impact probability computed in year t. The RR values may theoretically vary between 0 (if no GD is recorded in the tree-ring series) and infinite (if multiple GDs are recorded on a limited number of trees that intercept a limited number of potential trajectories; i.e. for low CIP values). We also employ the CIP to improve our tree selection. Accordingly, for scenarios S2-S5, trees located in the upper part of the slope and thus being the first to be impacted by rockfall, were extracted preferentially from dat2019 for scenarios S2-S5, whereas those located in the direct fall line of other trees (thereby protecting each other) were ignored.

3.4. Comparison of sampling strategies and analysis of meteorological data

The annual resolution of tree-ring series has so far limited the detection of meteorological drivers of rockfalls and has precluded any correlation with hourly-to-daily meteorological records. In order to fill this gap, we used re-analyses data from the SAFRAN meteorological downscaling and surface analysis system (Durand et al., 2009). This system performs an objective analysis of weather data available from various observation networks (including radar and satellite data) to provide freely available, continuous time series of meteorological variables

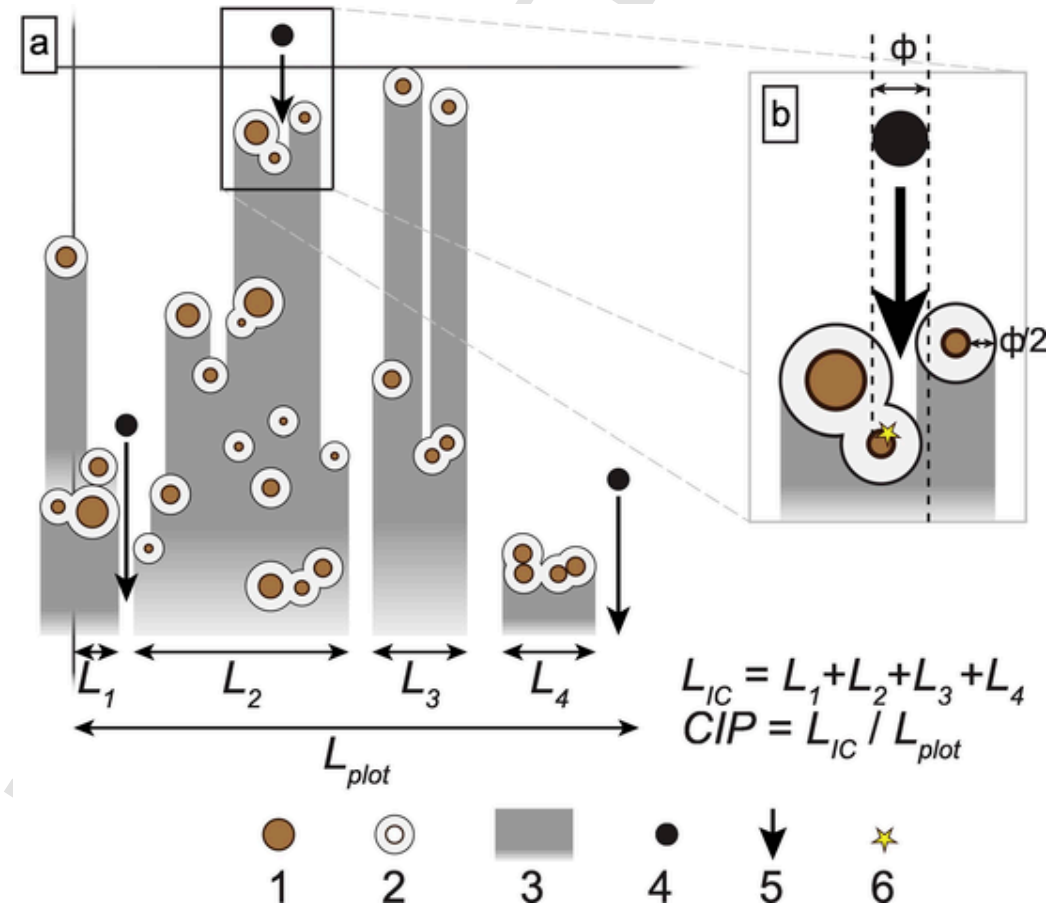

Fig. 3. a. Computation of the Conditional Impact Probability (CIP) taking into account the distribution of trees within the plot b. Computation of impact circles. 1. Tree stem; 2. Circle of impact; 3. Projection of the circles of impacts to the bottom boundary of the cell analyzed; 4. Rock of a given diameter; 5. Trajectory of the falling rock; 6. Rockfall impact. L1, L2, L3 and L4 are the widths of the projection of the circles of impact at the bottom of the cell. L_{plot} is the width of the analyzed cell. Adapted from Favillier et al. (2017).

at hourly resolution, for elevation steps of 300 m, different slope aspects and angles within massifs, and therefore for horizontally and climatologically homogeneous regions (Lafaysse et al., 2013; Vernay et al., 2019).

In the context of this study, we extracted hourly-resolved time series of temperature, precipitation totals and freeze–thaw cycles (1959–2017) from SAFRAN. Correlations between reconstructed rockfall activity obtained for scenarios S1-S6 and SAFRAN time series were tested for all variables averaged over one and up to 36 (~1 year) ten-day windows starting on October 1–10 (in year n-1 preceding the growing season) and ending in September 21–30 (in year n).

Delonca et al. (2014) and D'Amato et al. (2016) synthesized meteorological parameters susceptible to trigger rockfall events. In calcareous regions, rainfall duration and intensities were found to increase pressure in rock joints, whereas freeze–thaw cycles favor through wedging while sunshine enhances thermal stress which in turn facilitates propagation of cracks. Considering typical timeframes operating on these triggers, 10-day to annual series (i.e. 360 days, or 36 ten-day series) of (1) precipitation sums, (2) number of rainfall events >10 and 20 mm day^{-1}, (3) minimum, (4) mean, and (5) maximum air temperatures, (6) variations thereof, (7) the absolute number of freeze thaw cycles (defined as the number of days in which Tmax > 0 °C and Tmin < 0 °C) as well as (8) minimum temperatures (-3 and −5 °C) and (9) daily variations of temperatures (+6 and +10 °C) have been extracted from the SAFRAN database for the period 1958–2017. Relationships between rockfall activity and meteorological parameters were analyzed in a four-step procedure. In a first step, Pearson correlation coefficients were calculated between reconstructed rockfall activity and variables (1–9) for periods ranging from 1 to 36 consecutive ten-day periods. All datasets were transformed to z-scores summarizing anomalies below or above the average, over the period 1958–2017, before correlation analyses were performed. The statistical significance of results was then tested with a one-tailed t-test at a significance level $\alpha = 0.05$.

4. Results

4.1. Reconstruction of rockfall activity based on different sampling strategies

The results of the rockfall reconstructions derived from scenarios S1-S6 scenarios are synthesized in Table 1.

In scenario S1 (Fig. 4 growth disturbances (GD) were identified for the periods 1840–2017 and 1959–2017, respectively. According to the Mann–Kendall analysis computed for the period 1959–2017 covered by the SAFRAN meteorological dataset, a linear monotonic increasing trend (significant at $p < 0.01$) exists for most of the time periods considered in Fig. 5a, with the exception of the time after 1987. Maximum rockfall activity (n > 10 GDs) is observed in 2013, 2012, 2007, 2002, 2000, 2005, 1997, 2016, 1976, 2008, and 2010.

In scenario S2, 477 and 446 GDs were retrieved from the 179 trees sampled in the entire plot over the period 1906–2017 and 1959–2017, respectively. Here, the CIP sharply increased from 18% in 1907 to 89% in 2017 and from 41 to 89% for the period 1959–2017. After correction of the data with the CIP, maximum rockfall activity is reconstructed in 2012, 1999, 2013, 2008, 2002 and 2010 (Fig. 4b). Rockfall frequency increased from 55 to 145 GD $decade^{-1}$ between 1959–1988 and 1989–2017, respectively. The linear trends detected with the Mann–Kendall test are comparable to scenario S1 and are not significant if analyses are restricted to a period starting in 1985 and extending to the present day (Fig. 5b).

Scenarios S3 and S4 include 108 (0.45 ha) and 83 trees (0.17 ha) for which injuries are more frequently visible on the tree stems (Table 1, Fig. 4d). In these compartments, 374 (S3) and 309 (S4) rockfall events have been retrieved from the tree-ring series between 1845 and 2017, among which 345 (92%, S3) and 293 (95%, S4) occurred since 1959. The potentially missed events decreased from 72% in 1959 to less than 7% in 2017 in S3 (Fig. 4c) and from 82 to 5% over the same period in S4 (Fig. 4d). Extreme rockfall activity was observed in 2002, 2008, 2010, and 2013 in both compartments. The reconstructions show the largest increasing trends (+0.4 events $year^{-1}$) for starting years ranging between 1959 and 1967 and ending years from 2008 to 2017. By contrast, if reconstructions only start after 1978 (S3) and 1972 (S4), respectively, rockfall activity becomes stationary (Fig. 5c,d).

According to the initial maps (Fig. 1d), rockfall activity is less frequent in the southern compartment of the plot considered in S5. In this scenario, 74 trees were included in the rockfall reconstruction. In total, 111 GDs were identified in the cores, mostly after 1959 (97 GDs, 88%). Decadal frequencies (22 GD $decades^{-1}$ over the period 1959–2017) confirm the rather limited rockfall activity that was estimated on the basis of a visual inspection of tree stems in the field. Trends over the 1959–2017 period are weak (ranging between −0.1 and + 0.1 event $year^{-1}$), irrespective of the period considered (Fig. 5e).

Finally, in S6, 137 GDs were retrieved from the analyzed cross-sections since 1959, with most scars occurring after 1989 (n = 123). Since 1989, the decadal rockfall frequency in S6 was 2.03 events $decade^{-1}$ $tree^{-1}$ prior to CIP correction, which corresponds to more than twice the values computed for scenarios S1-S5 (with 0.42, 0.7, 0.9, 1.01, 0.37 events $decade^{-1}$ $tree^{-1}$, respectively). Noteworthy, in the case of scenario S6, the CIP remained low (<2%) until 1993 and only reached a value of 37.4% at the end of the reconstruction in 2017. Given the restricted length of the reconstruction, the Mann–Kendall test was not computed for scenario S6.

Fig. 6 synthesizes correlations between the reconstructions S1-S5 over the period 1959–2017 (a) and S1-S6 over the period 1989–2017 (b). For obvious reasons, highly significant positive correlations ($0.88 < r < 0.99$, $p < 0.01$) are computed between scenarios S2, S3 and S4, as they are partly based on the same trees for both periods. Correlations between scenario S1 and scenarios S2-S5 sharply increased after 1989 (0.41–0.64). Finally, and more interestingly, (1) correlations between the northern and southern compartments (S4-S5) of the slope, albeit significant ($p < 0.05$) since 1989, remain weak ($r < 0.42$). (2) Scenario S6 is negatively correlated ($p < 0.05$) with S3 and especially S4, although the cross-sections were cut in the upper part of the northern compartment as well.

4.2. Correlation between rockfall activity and meteorological covariates

Prior to correlation analyses, rockfall reconstructions and meteorological series were transformed into z-scores for the period covered by meteorological time series (1959–2017). According to the Mann–

Table 1
Overview of sampling strategy scenarios.

Scenario	Area	Nb of trees	Conifers (%)	Broadleaved (%)	Nb of GD	CIP 2017	Reliability	Surface (ha)
S1	Entire slope	161	62	38	326	No CIP	Unknown	1.04
S2	Entire slope	179	59	41	477	0.89	1969–2017	0.81
S3	N. compartment	108	73	27	374	0.93	1980–2017	0.45
S4	Upper N. compartment	83	75	25	309	0.86	1989–2017	0.17
S5	S. Compartment	71	31	69	111	0.79	1960–2017	0.36
S6	Cross Sections	24	67	33	137	0.37	/	0.28

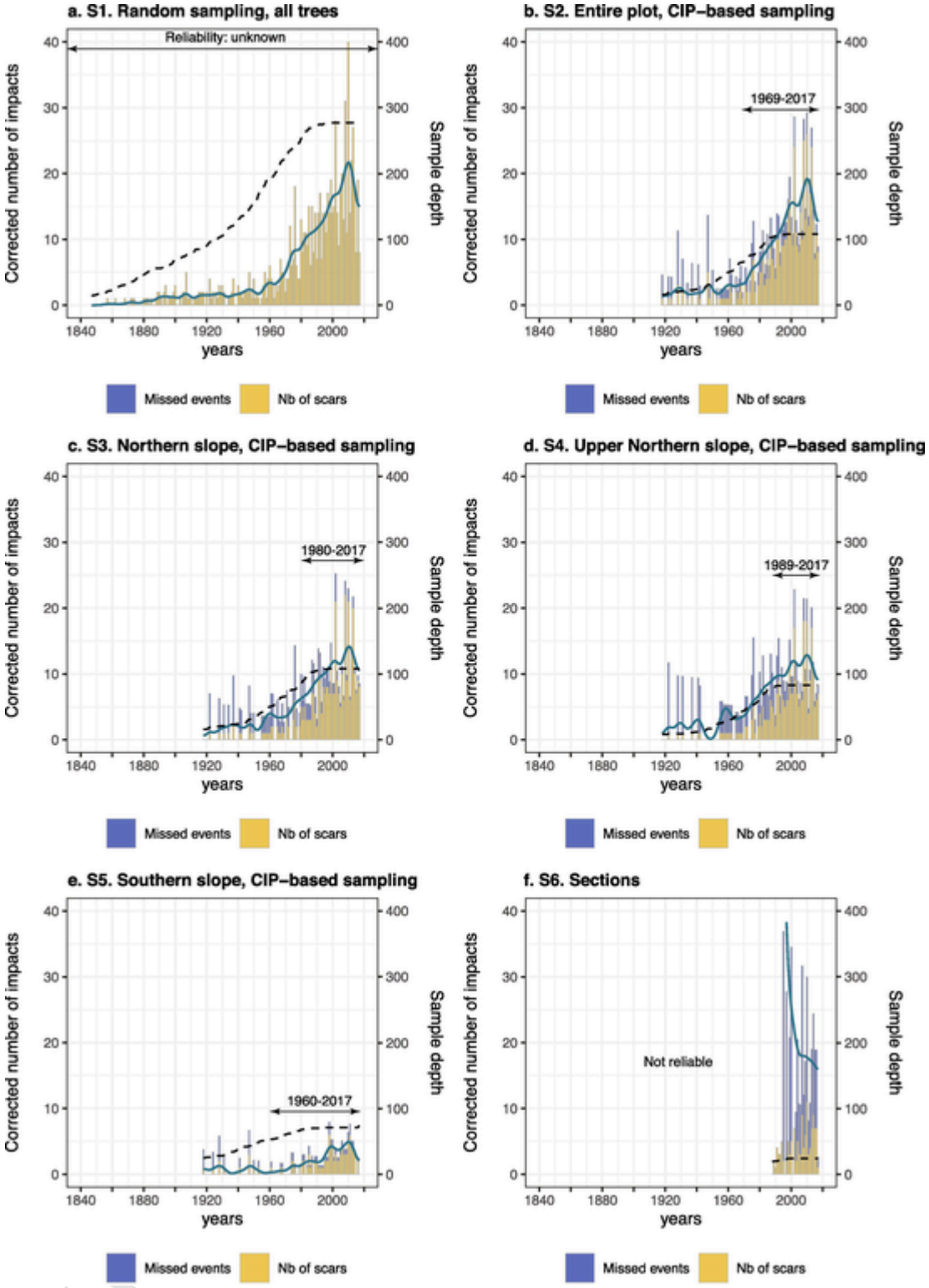

Fig. 4. Variations of rockfall activity reconstructed from sampling scenarios S1-S6 (a-f). Yellow bars represent the total number of GDs while blue bars represent the missed events considering the CIP. A 10-yr lowpass filter has been used to emphasize decadal fluctuations of rockfall activity (blue solid line). The black dashed line represents the variation of the sample depth over time. (For interpretation of the references to colour in this figure legend, the reader is referred to the web version of this article.)

Kendall test, the reconstructions derived from each scenario are stationary after 1989. Therefore, correlations between rockfall activity and meteorological data were computed separately for the full period covered by the SAFRAN re-analysis data (1959–2017) (Fig. 7a) and for the sub-period 1989–2017 (Fig. 7b) for which no significant trend in rockfall activity was observed in the tree-ring records. Interestingly, no significant correlation ($p < 0.01$) was found between the chronologies computed for the six scenarios, temperature (minimum, mean, maximum), or freeze–thaw cycles, irrespective of the period considered.

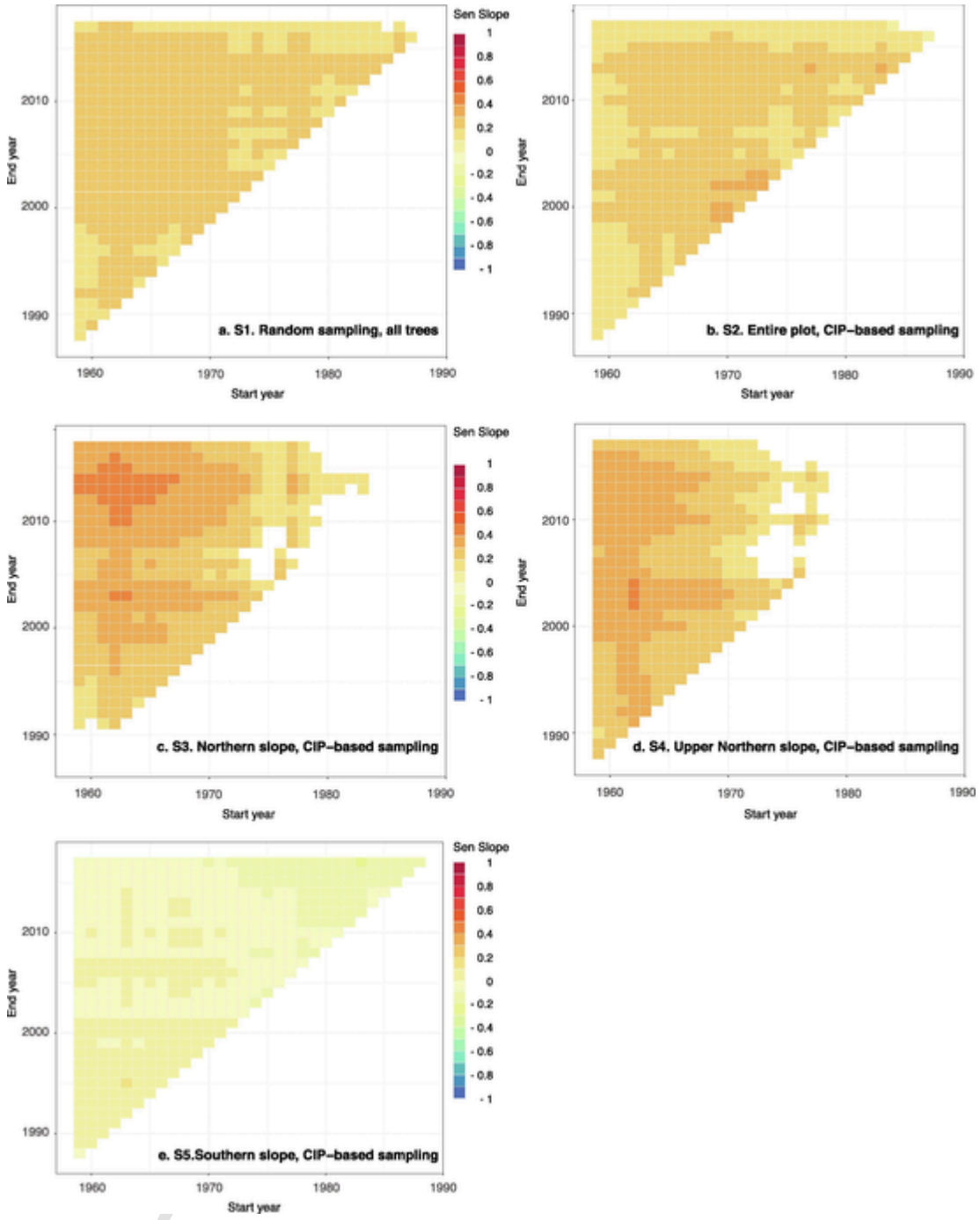

Fig. 5. Linear monotonic trends (Theil-Sen slope) detected in tree-ring reconstructions of rockfall activity. The significance of the trend ($p < 0.01$) was tested with the Mann–Kendall test for sampling scenarios S1-S5 (a-e). For each scenario, the MK test was computed over the 1959–2017 period for which meteorological records exist, using moving time windows with lengths varying from 30 to 59 years. Start years (x-axis) range from 1959 to 1988, whereas end years (y-axis) are comprised between 1988 and 2017.

By contrast, and in the case of precipitation totals, results differ according to the period analyzed and the six sampling scenarios (Fig. 7a, b). As a rule, correlations between rockfall reconstructions and precipitation totals computed over the period 1959–2017 (Fig. 7a) are weaker than those computed for 1989–2017. In addition, and irrespective of the scenario considered, meteorological drivers of rockfall activity differ over both periods. Between 1989 and 2017, we do not find any significant correlation between precipitation and rockfall in the southern compartment (S5) or in the northern sector for which cross-sections have been taken (S6). By contrast, in the case of scenario S1, derived from random sampling strategy, we obtain negative correlations ($r = -0.5$, $p < 0.01$) with winter precipitation.

In the case of the CIP-based rockfall reconstructions computed for the entire plot (S2) and the (upper) northern (S3-S4) compartments, fall and winter precipitation totals summed over 10–13 consecutive ten-day periods centered around December 1–10 (n-1) show the largest influence on inter-annual variations of rockfall ($0.35 > r > 0.25$, $p < 0.01$) over the period 1959–2017, whereas more robust correlations ($r > 0.5$, $p < 0.01$) are obtained with summer (from June 1–10 (n) to September 1–10 (n)) precipitation between 1989 and 2017. For this period, maximum correlations ($r = 0.58$, 0,65, 0.68 for S2, S3 and S4, re-

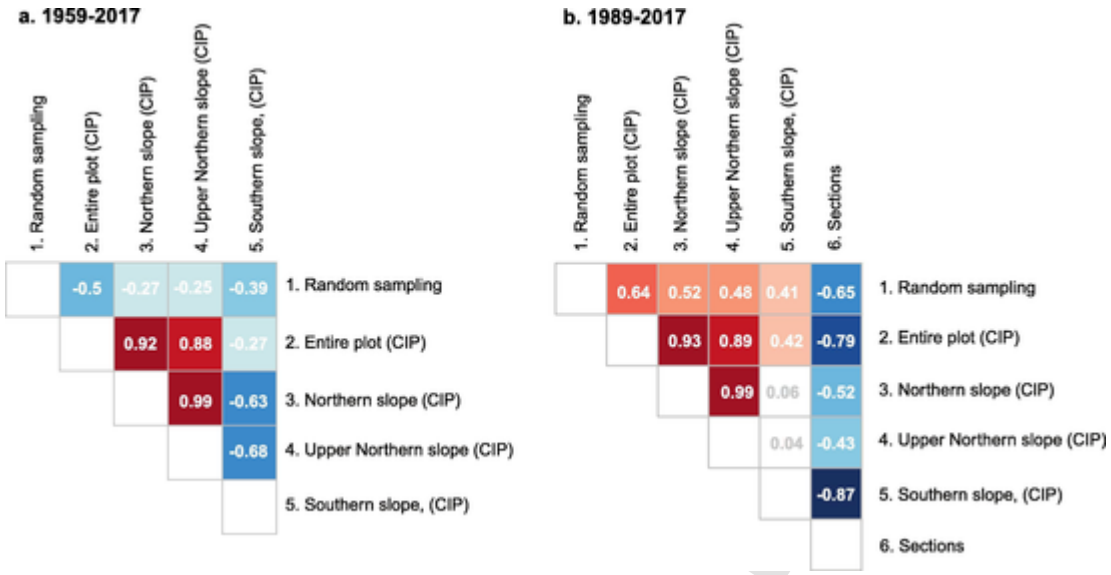

Fig. 6. Correlation matrices obtained for reconstructions based on the different scenarios and computed over the periods 1959–2017 (S1-S5, a) and 1989–2017 (S1-S6, b). Red and blue shades represent positive and negative correlation values significant at $p < 0.05$, respectively. Insignificant values ($p > 0.05$) are indicated in grey. (For interpretation of the references to colour in this figure legend, the reader is referred to the web version of this article.)

spectively) are computed with precipitation totals computed over 5 consecutive ten-day windows centered on August 11–20 (n) (Fig. 7b). Fig. 9 represents the regression of these precipitation totals over the rockfall reconstruction for S2 (Fig. 9a), S3 (Fig. 9b) and S4 (Fig. 9c), for the 1989–2017 period, and does not contain significant outliers that could have biased r values. Correlations between meteorological variables and rockfall reconstructions S2-S4, computed over the period 1959–2017 and moving time windows with lengths varying from 30 to 59 years are presented in Fig. 8. For all three scenarios, correlations increase if the time windows starts after 1973, and higher r-values (0.74, 0.73 and 0.77, $p < 0.01$ for S2, S3, S4, respectively) are computed for the period 1980–2009. Interestingly, correlations are significant over a longer period (1964–2017) between summer rainfall totals and rockfall reconstructions S3-S4 when compared to reconstruction S2 (1971–2017).

5. Discussion

5.1. How to improve sampling strategies aimed at reconstructing rockfall?

On forested slopes, growth disturbances in trees are reliable ecological indicators of past rockfall activity and fluctuations thereof over decadal to centennial timescales (Alestalo, 1971; Stoffel et al., 2010; Bollati et al., 2018). Yet, apart from Perret et al. (2006), Šilhán et al. (2011), Zielonka and Wronska-Walach (2019) and Mainieri et al. (2020), reconstructed time series of rockfall were only rarely compared to instrumental data with the aim to detect meteorological drivers of process activity and fluctuations in activity. This lack of dendrogeomorphic studies looking at actual drivers of rockfall activity is attributed (1) to the presence of non-climatic trends in reconstructions that can be intrinsic to the dendrogeomorphic approach and (2) to the absence of clear guidelines regarding sampling design that would allow obtaining robust relations between rockfall activity reconstructed from tree rings and the assessment of meteorological drivers of activity. In this context, the present study aimed at showing potential impacts of different sampling designs on the detection and identification of meteorological drivers of past rockfalls as reconstructed from tree-ring series. The study capitalizes on the CIP approach (Moya et al., 2010; Trappmann et al., 2014; Trappmann and Stoffel, 2015) to optimally quantify uncertainties inherent to tree-ring reconstructions.

Comparing the six chronologies developed at the Saint-Guillaume study plot, we clearly demonstrate the influence of sampling patterns on resulting reconstructions. Significant differences are thus observed, at the slope scale, between reconstructions obtained through random sampling and those selecting trees based on the CIP approach. Despite the wide spectrum of meteorological variables tested in this study, we failed to identify robust meteorological drivers of rockfall activity in reconstruction S1 where a random sampling across the slope was implemented. By contrast, in reconstructions S2-S4, where injured trees were selected on the basis of the CIP approach, summer precipitation totals explain almost half of the inter-annual rockfall variability over the last three decades. This study therefore highlights the added value of high-resolution maps of the study plot as they can facilitate the implementation of reliable sampling strategies and a targeted selection of trees. Similarly, clear differences exist between the northern and southern compartments of the slope in terms of (1) rockfall frequency as illustrated by the preliminary maps, (2) inter-annual variations as revealed by weak, poorly significant correlations between reconstructions S3-S4 and S5 as well as (3) relations to meteorological variables. Such differences can be attributed to differences in rockfall activity but also reflect the uneven distribution of conifer and broadleaved trees with different growth rates, heights and diameters (Mainieri et al., 2019a) between the compartments. More specifically, we show that interspecific differences could result in a greater difficulty to retrieve healed injuries in broadleaved trees (Arbellay et al., 2012) than in conifer species for which TRDs, with a tangential spread of resin ducts on more than one-third of stem circumference, allow overcoming the problem of masked scars (Schneuwly et al., 2009). We thus hypothesize that the rather moderate rockfall activity with weak inter-annual variations, combined with the complexity to retrieve scars from broadleaved trees (Martin-Benito et al., 2013; Favillier et al., 2017; Mainieri et al., 2019a), has prevented us to derive a more solid definition of meteorological drivers in reconstruction S5. In other words, our results suggest that a precise identification of homogeneous areas in terms of rockfall activity and forest stand structure is crucial for a clear detection of meteorological drivers. Finally, comparable results are obtained from reconstruction S3 (108 trees) located within the entire northern compartment of the plot (0.81 ha) and reconstruction S4 which was based on only 71 trees from the upper portion of the same compartment (0.45). Moreover, we failed to demonstrate the added-value of reconstruction S6 which was based on a systematic, destructive sampling of cross-sections (rather than relying on increment cores). Even if reconstruction S6 yields a higher overall frequency of events and is theoretically free

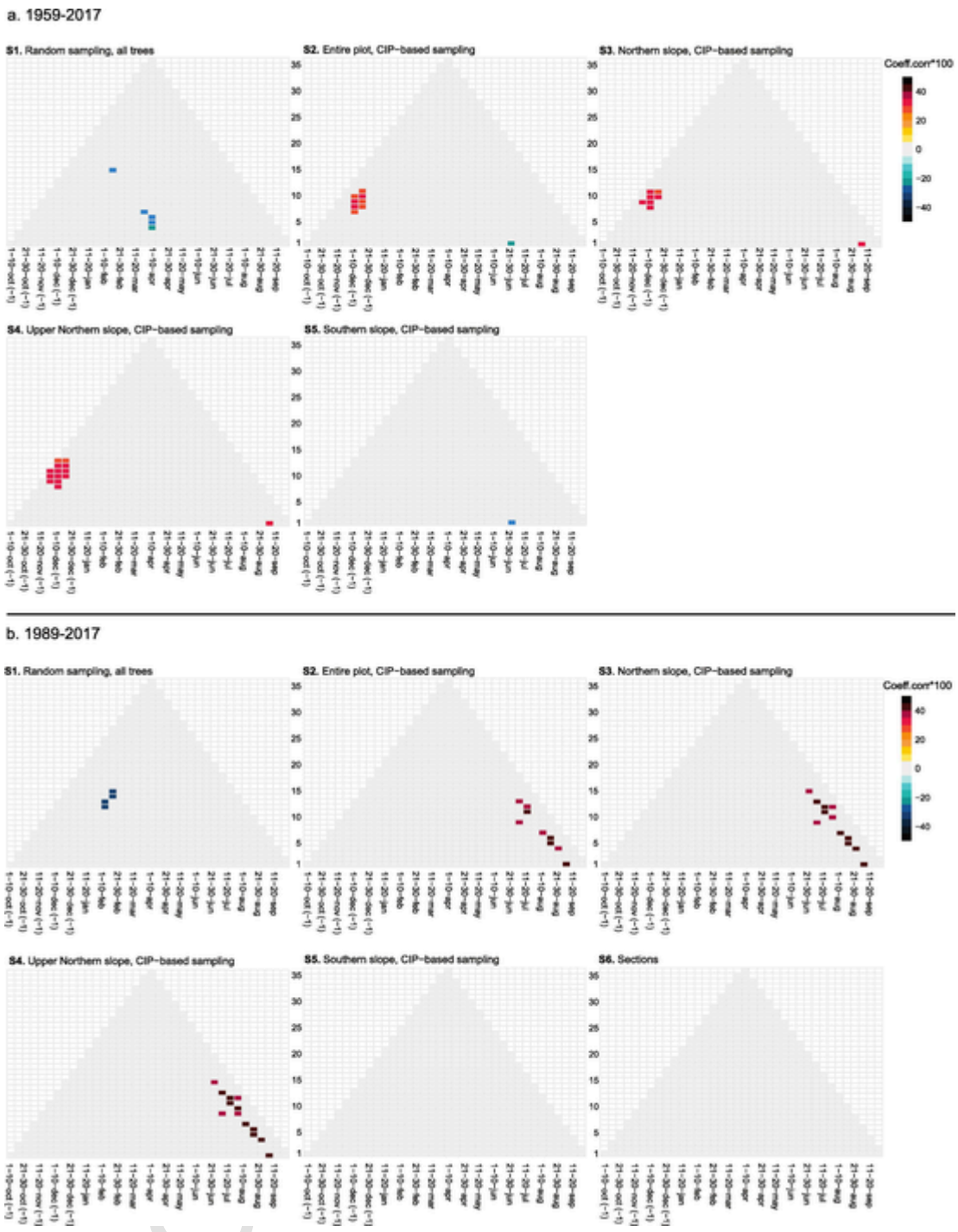

Fig. 7. Correlations between reconstructions derived from scenarios S1-S6 and precipitation totals computed over 1 to 36 consecutive 10-day periods extending from October 1–10 in the year preceding tree-ring formation (n-1) to September 21–30 of the current year (n). All mapped correlations are significant at $p < 0.05$.

from biases related to masked scars, its reliability seems to remain hampered by its limited spatial fingerprint. As a consequence, and in order to increase the cost-benefit ratio of future dendrogeomorphic studies aimed at detecting meteorological drivers, we recommend (1) to limit the downslope extent of plots while increasing their width, as previously suggested by Gsteiger (1993) and (2) to core the first rows of trees below cliffs more systematically, provided that its trees are old enough to enable multidecadal reconstruction, as they are located next to the cliffs and will therefore act as a first line of defense recording rockfall (Perret et al., 2006).

5.2. Stationarity of the reconstructions and detection of meteorological drivers

Despite the precise quantification of the CIP back in time and its application to estimate missed events in the six rockfall chronologies developed within the Saint-Guillaume plot, we still find marked and increasing trends over the period 1959–2017. More precisely, significant increasing trends in rockfall activity have been detected until 1987, 1984, 1978 and 1974 for S1-S4, respectively (Fig. 5). Despite the stringency of our approach, we explain these trends by the persistence of bi-

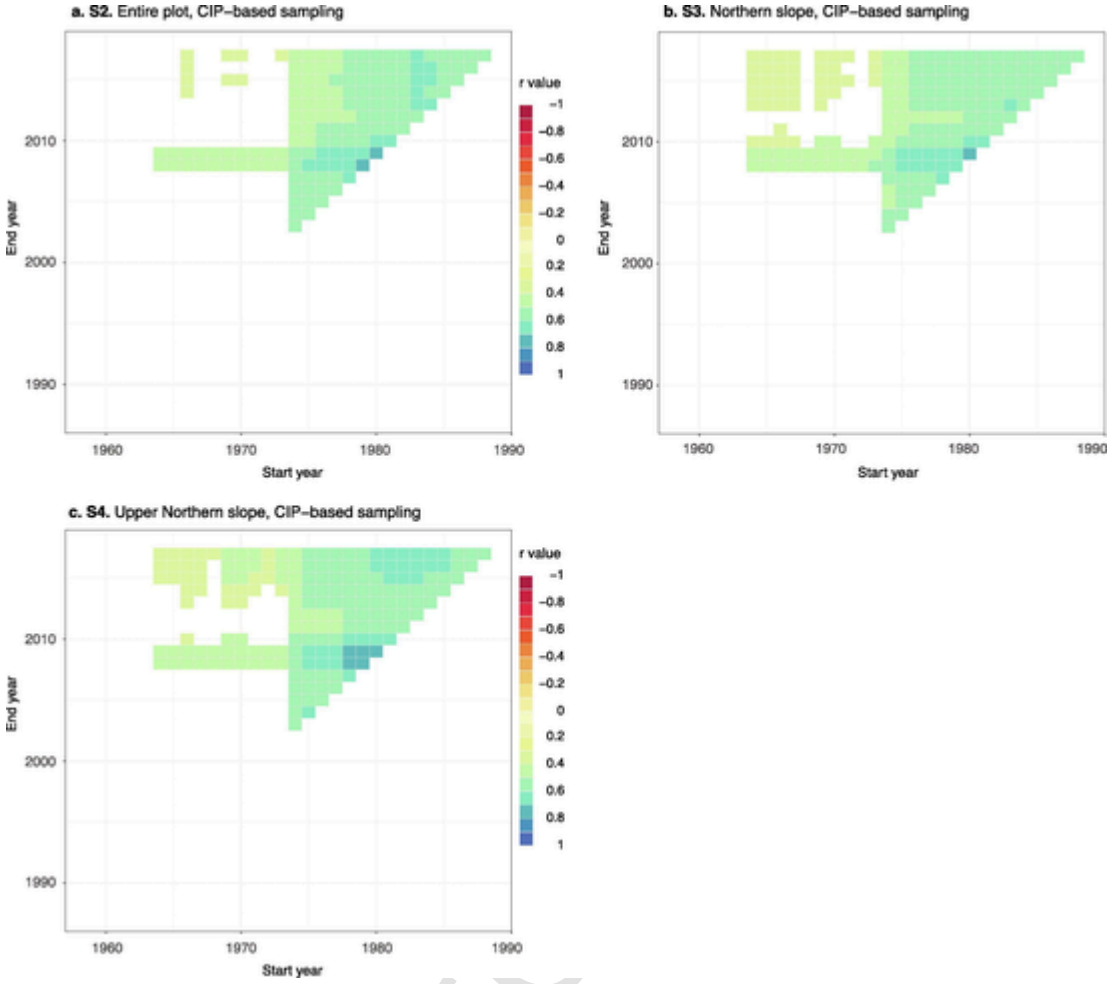

Fig. 8. Correlation between rockfall reconstructions computed from CIP-based sampling scenarios S2 (a), S3 (b), S4 (c) and precipitation totals computed over 5 consecutive 10-day periods centered around August 11–20 (n). Only r values significant at $p < 0.01$ are shown. For each scenario, r and p-values were computed over the period 1959–2017 covered by meteorological series, as well as for moving time windows with lengths varying from 30 to 59 years. Start years (x-axis) are between 1959 and 1988, end years (y-axis) between 1988 and 2017.

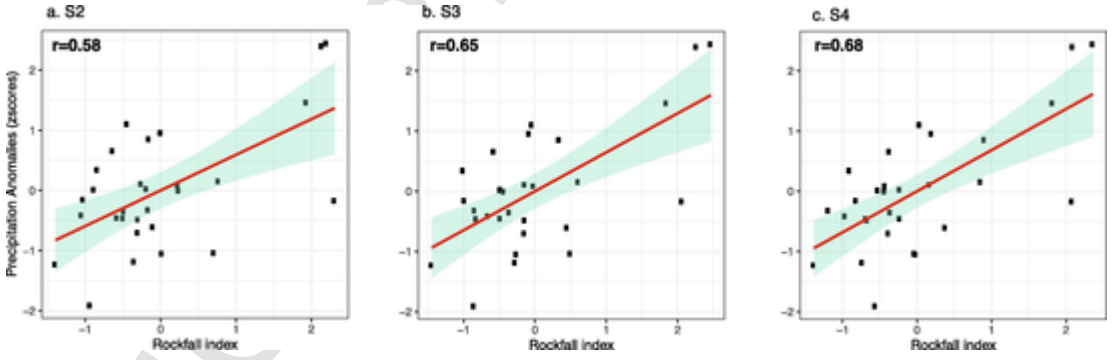

Fig. 9. Linear regression between rockfall reconstructions computed from scenarios S2 (a), S3 (b), S4 (c) and precipitation totals computed over 5 consecutive 10-day periods centered around August 11–20 (n) for the period 1989–2017.

ases intrinsic to dendrogeomorphic approaches, such as the difficulty of identifying older, overhealed scars on stems (Schneuwly et al., 2009), the changing sensitivity of trees to record impacts with increasing age (Šilhán et al., 2013), or the fact that different tree species will not record scars the same way (i.e. different energies needed to inflict scars depending on bark thickness, for instance (Favillier et al., 2017; Trappmann et al., 2013)). Interestingly, higher correlations were computed between the different reconstructions and precipitation totals computed over five consecutive ten-day periods centered around August 11–20 for the periods 1987–2019 (S1), 1984–2019 (S2), 1978–2019 (S3), and 1974–2019 (S4). In the past, various thresholds have been defined either empirically or arbitrary to limit rockfall reconstructions in time or to evaluate the temporal reliability of reconsructions. These thresholds consisted of (1) a minimum number of trees sampled (Perret et al., 2006; Schneuwly and Stoffel, 2008a; Schneuwly and Stoffel, 2008b; Šilhán et al., 2013), (2) trees that were homogeneously distributed on the slope (Stoffel et al., 2005), (3) a minimum exposed diameter (Šilhán et al., 2011), (4) an abrupt change in the annual frequency of rockfalls (Moya et al., 2010) or (5) a 0.5 CIP value (Trappmann et al., 2013; Morel et al., 2015). Our results

suggest that the Mann–Kendall test could be used to quantify the robustness of rockfall reconstructions more objectively and to overcome the rather arbitrary thresholds used in the past.

5.3. Meteorological drivers of rockfall activity from a non-glaciated calcareous cliff of the French Alps

Despite the limited length for which the reconstructions presented in this study are reliable, we would like to stress that our records still exceeds the length of virtually all other inventories available for the (French) Alps. In addition, the efforts deployed to quantify uncertainties ultimately increases confidence and the robustness of our findings regarding meteorological drivers of rockfall at Saint-Guillaume. Comparison between our CIP-based rockfall reconstructions and meteorological parameters derived from the SAFRAN re-analyses datasets demonstrates that spring and – even more so – rainfall totals during summer were the main drivers of inter-annual fluctuations in rockfall activity at the study site over the last decades. Correlations between rockfall activity and precipitation totals computed over 5 consecutive ten-day windows centered on August 11–20 (n) exceed 0.5 since 1975 in scenarios S2-S4 and even reach 0.6 if the period is restricted to 1989–2017 (Fig. 8). Although correlations do not allow determination of thresholds for the actual triggering of rockfall, our results still agree with findings of D'Amato et al. (2016) who report, based on a 2.5 year LiDAR survey of the calcareous Saint-Eynard cliff (Chartreuse Massif, 30 km northeast from Saint-Guillaume), that rockfall frequency could be multiplied by a factor of 26 if mean rainfall intensity exceeds 5 mm h^{-1}. They attribute the increasing rockfall frequency after rainfall episodes to the chemical weathering (including limestone dissolution) of the thin marly layers present at their site. Our study also converges with findings from the Bavarian Alps (Krautblatter and Moser, 2009) where a 5-yr record of rock fragments found in traps shows that 90% of all small-magnitude rockfalls were triggered by rainstorms. At larger scale, a similar dependency of rockfall from precipitation has been reported for non-glaciated cliffs in Burgundy (France; Delonca et al., 2014), the Tatras (Poland; Zielonka and Wronska-Walach, 2019), the Canadian Cordillera (Macciotta et al., 2015), Hong-Kong (Chau et al., 2003), the Tramuntana Range (Spain; Mateos et al., 2012) or the Japanese Alps (Matsuoka, 2019; Imaizumi et al., 2020). In the latter case, based on a coupled geomorphic and microclimatic monitoring, Matsuoka (2019) explains the increasing rockfall frequency by raised water pressure in rock joints or the lubrification of joints after rainfall. By contrast, correlation were neither significant with minimum, mean, maximum temperatures nor with freeze–thaw cycles, despite the wide spectrum of combinations tested (i.e. 1 to 36 consecutive 10-day periods for each meteorological variable). In that sense, our results differ from the other climate-rockfall assessments based on dendrogeomorphic reconstructions (Perret et al., 2006; Šilhán et al., 2011) and, in more general terms, from a large body of monitoring literature demonstrating that thermal conditions and especially freeze–thaw cycles would control rockfall frequency in mountainous regions (Matsuoka and Sakai, 1999; Frayssines and Hantz, 2006; D'Amato et al., 2016; Matsuoka, 2019). Several hypotheses may explain the absence of relationships between rockfall activity and thermal variables at Saint Guillaume, such as (1) the resolution of the dendrogeomorphic records which only partly represent rockfall activity and probably do not include high-frequency–low-magnitude events; (2) the complex influence of freeze–thaw cycles on rockfall activity, with events occurring more frequently during warming and thawing than during cooling periods (D'Amato et al., 2016) and under moisture-saturated freeze–thaw conditions (Krautblatter and Moser, 2009); or (3) the use of the SAFRAN re-analysis dataset which does not reflect microclimatic variations and effects related to microtopography of cliffs (Matsuoka and Sakai, 1999; Schneuwly and Stoffel, 2008b; Perret et al., 2006; Matsuoka, 2019; Zielonka and Wronska-Walach, 2019).

6. Conclusions

In this paper, we used the extensive dataset computed by Mainieri et al. (2019a) to quantify potential biases in tree-ring based rockfall reconstructions back in time, as well as to evaluate impacts of different sampling strategies on the detection of meteorological drivers of rockfall activity. In methodological terms, we demonstrate that (i) carefully selecting trees with the conditional impact probability, (ii) together with a preference for the selection of trees in more active compartments of the study plot as well as (iii) at the contact of the slope with the cliff will significantly increase the quality of the reconstruction and ease its comparison with meteorological variables. In addition, given enhanced correlations between tree-ring records and meteorological parameters in the absence of multi-decadal linear trends, we also recommend using the Mann–Kendall test to quantify the robustness of reconstructions more objectively in the future. Once the above-mentioned criteria are considered, relationships between reconstruction S4 and meteorological variables computed over 10 to 36 consecutive 10-day periods enabled identification of summer precipitation totals as the major driver of inter-annual rockfall fluctuations reconstructed at Saint-Guillaume. Yet, and despite the stringency of the procedure developed here, we did not find any statistically significant correlation between rockfall activity and thermal variables (especially with freeze–thaw cycles), even if these have been demonstrated as a key triggering factor of rockfalls in calcareous cliffs located at comparable altitudes. We explain this limited correlation mostly by complex relationships between moisture, freezing and rockfall events. Yet, we plead for more systematic coupling between dendrogeomorphic studies and rockfall as well as microclimatic monitoring of sites in the future to validate these hypotheses.

Declaration of Competing Interest

The authors declare that they have no known competing financial interests or personal relationships that could have appeared to influence the work reported in this paper.

Acknowledgements

This research benefited from the support of the national C2ROP project supported by MEDDE, the Ministry of Ecology, Sustainable Development and Energy (http://www.c2rop.fr/) and of Labex OSUG@2020 and within the CDP-Trajectories framework, of the French National Research Agency (ANR-15-IDEX-02). The authors declare no conflicts of interest. We gratefully thank the reviewers for their valuable comments that helped to improve and to clarify our manuscript.

References

Alestalo, J., 1971. Dendrochronological interpretation of geomorphic processes. Fennia - Int. J. Geogr. 105 (1) https://fennia.journal.fi/article/view/40757.

Arbellay, E., Corona, C., Stoffel, M., Fonti, P., Decaulne, A., 2012. Defining an adequate sample of earlywood vessels for retrospective injury detection in diffuse-porous species. PLoS ONE 7 (6), e38824 https://dx.plos.org/10.1371/journal.pone.0038824.

Bannan, M.W., 1936. Vertical resin ducts in the secondary wood of the Abietineae. New Phytol. 35 (1), 11–46 http://doi.wiley.com/10.1111/j.1469-8137.1936.tb06864.x.

Birsan, M.-V., Molnar, P., Burlando, P., Pfaundler, M., 2005. Streamflow trends in Switzerland. J. Hydrol. 314 (1–4), 312–329 https://linkinghub.elsevier.com/retrieve/pii/S0022169405002970.

Bollati, I., Crosa Lenz, B., Golzio, A., Masseroli, A., 2018. Tree rings as ecological indicator of geomorphic activity in geoheritage studies. Ecol. Ind. 93, 899–916 https://linkinghub.elsevier.com/retrieve/pii/S1470160X18303947.

Bräker, O.U., 2002. Measuring and data processing in tree-ring research – a methodological introduction. Dendrochronologia 20 (1–2), 203–216 https://linkinghub.elsevier.com/retrieve/pii/S112578650470017X.

Chau, K.T., Wong, R.H.C., Liu, J., Lee, C.F., 2003. Rockfall Hazard Analysis for Hong Kong Based on Rockfall Inventory. Rock Mech. Rock Eng. 36 (5), 383–408 http://link.springer.com/10.1007/s00603-002-0035-z.

Corona, C., Lopez-Saez, J., Favillier, A., Mainieri, R., Eckert, N., Trappmann, D., Stoffel, M., Bourrier, F., Berger, F., 2017. Modeling rockfall frequency and bounce height

from three-dimensional simulation process models and growth disturbances in submontane broadleaved trees. Geomorphology 281, 66–77 https://linkinghub.elsevier.com/retrieve/pii/S0169555X16304639.
D'Amato, J., Hantz, D., Guerin, A., Jaboyedoff, M., Baillet, L., Mariscal, A., 2016. Influence of meteorological factors on rockfall occurrence in a middle mountain limestone cliff. Nat. Hazards Earth Syst. Sci. 16 (3), 719–735 https://www.nat-hazards-earth-syst-sci.net/16/719/2016/.
Delonca, A., Gunzburger, Y., Verdel, T., 2014. Statistical correlation between meteorological and rockfall databases. Nat. Hazards Earth Syst. Sci. 14 (8), 1953–1964 https://www.nat-hazards-earth-syst-sci.net/14/1953/2014/.
Dorren, L., Berger, F., Jonsson, M., Krautblatter, M., Mölk, M., Stoffel, M., Wehrli, A., 2007. State of the art in rockfall – forest interactions. Schweizerische Zeitschrift fur Forstwesen 158 (6), 128–141 http://szf-jfs.org/doi/abs/10.3188/szf.2007.0128.
Dorren, L.K., Berger, F., le Hir, C., Mermin, E., Tardif, P., 2005. Mechanisms, effects and management implications of rockfall in forests. For. Ecol. Manage. 215 (1–3), 183–195 https://linkinghub.elsevier.com/retrieve/pii/S0378112705003324.
Dorren, L.K.A., Berger, F., Putters, U.S., 2006. Real-size experiments and 3-D simulation of rockfall on forested and non-forested slopes. Nat. Hazards Earth Syst. Sci. 6 (1), 145–153 http://www.nat-hazards-earth-syst-sci.net/6/145/2006/.
Durand, Y., Laternser, M., Giraud, G., Etchevers, P., Lesaffre, B., Mérindol, L., 2009. Reanalysis of 44 Yr of Climate in the French Alps (1958–2002): Methodology, Model Validation, Climatology, and Trends for Air Temperature and Precipitation. J. Appl. Meteorol. Climatol. 48 (3), 429–449 http://journals.ametsoc.org/doi/abs/10.1175/2008JAMC1808.1.
Dussauge-Peisser, C., 2002. Evaluation de l'aléa éboulement rocheux: développements méthodologiques et approches expérimentales; application aux falaises calcaires du Y grenoblois. Grenoble 1 URL http://www.theses.fr/2002GRE10052.
Eckert, N., Mainieri, R., Bourrier, F., Giacona, F., Corona, C., Le Bidan, V., Lescurier, A., 2020. Une base de données événementielle du risque rocheux dans les Alpes Françaises. Revue Française de Géotechnique 163, 3 https://www.geotechnique-journal.org/10.1051/geotech/2020012.
Erismann, T.H., Abele, G., 2001. Dynamics of Rockslides and Rockfalls. Springer Berlin Heidelberg, Berlin, Heidelberg http://link.springer.com/10.1007/978-3-662-04639-5.
Favillier, A., Lopez-Saez, J., Corona, C., Trappmann, D., Toe, D., Stoffel, M., Rovéra, G., Berger, F., 2015. Potential of two submontane broadleaved species (Acer opalus, Quercus pubescens) to reveal spatiotemporal patterns of rockfall activity. Geomorphology 246, 35–47 https://linkinghub.elsevier.com/retrieve/pii/S0169555X15300283.
Favillier, A., Mainieri, R., Saez, J.L., Berger, F., Stoffel, M., Corona, C., 2017. Dendrogeomorphic assessment of rockfall recurrence intervals at Saint Paul de Varces. Western French Alps. Géomorphologie: relief, processus, environnement 23 (2).
Ferrari, F., Giacomini, A., Thoeni, K., 2016. Qualitative Rockfall Hazard Assessment: A Comprehensive Review of Current Practices. Rock Mech. Rock Eng. 49 (7), 2865–2922 http://link.springer.com/10.1007/s00603-016-0918-z.
Frayssines, M., Hantz, D., 2006. Failure mechanisms and triggering factors in calcareous cliffs of the Subalpine Ranges (French Alps). Eng. Geol. 86 (4), 256–270 https://linkinghub.elsevier.com/retrieve/pii/S0013795206001700.
Gardner, J., 1970. Rockfall: a geomorphic process in high mountain terrain. The Albertan Geographer 6, 15–20.
Gsteiger, P., 1989. Steinschlag, Wald, Relief: empirische Grundlagen zur Steinschlagmodellierung. na, google-Books-ID: 3cgESwAACAAJ.
Gsteiger, P., 1993. Steinschlagschutzwald. Ein Beitrag zur Abgrenzung, Beurteilung und Bewirtschaftung. Schweizerische Zeitschrift für Forstwesen 144 (2), 115–132.
Hantz, D., Vengeon, J.M., Dussauge-Peisser, C., 2003. An historical, geomechanical and probabilistic approach to rock-fall hazard assessment. Nat. Hazards Earth Syst. Sci. 3 (6), 693–701 http://www.nat-hazards-earth-syst-sci.net/3/693/2003/.
Helsel, D. R., Hirsch, R., 1992. Statistical Methods in Water Resources. In: Studies in Environmental Science. Vol. 49. Elsevier, pp. v–vi. URL https://linkinghub.elsevier.com/retrieve/pii/S0166111608710987
Šilhán, K., Brázdil, R., Pánek, T., Dobrovolný, P., Kašicková, L., Tolasz, R., Turský, O., Václavek, M., 2011. Evaluation of meteorological controls of reconstructed rockfall activity in the Czech Flysch Carpathians: evaluation of meteorological controls of rockfall activity. Earth Surf. Proc. Land. 36 (14), 1898–1909 http://doi.wiley.com/10.1002/esp.2211.
Šilhán, K., Pánek, T., Hradecký, J., 2013. Implications of spatial distribution of rockfall reconstructed by dendrogeomorphological methods. Nat. Hazards Earth Syst. Sci. 13 (7), 1817–1826 https://www.nat-hazards-earth-syst-sci.net/13/1817/2013/.
Imaizumi, F., Trappmann, D., Matsuoka, N., Ballesteros Cánovas, J.A., Yasue, K., Stoffel, M., 2020. Interpreting rockfall activity on an outcrop–talus slope system in the southern Japanese Alps using an integrated survey approach. Geomorphology 371, 107456 http://www.sciencedirect.com/science/article/pii/S0169555X20304293.
Kellerer-Pirklbauer, A., Rieckh, M., 2016. Monitoring nourishment processes in the rooting zone of an active rock glacier in an alpine environment. Zeitschrift für Geomorphologie, Supplementary Issues 60 (3), 99–121 http://openurl.ingenta.com/content/xref?genre=article&issn=1864-1687&volume=60&issue=3&spage=99.
Krautblatter, M., Moser, M., 2009. A nonlinear model coupling rockfall and rainfall intensity based;≠ wline on a four year measurement in a high Alpine rock wall (Reintal, German Alps). Nat. Hazards Earth Syst. Sci. 9 (4), 1425–1432 https://www.nat-hazards-earth-syst-sci.net/9/1425/2009/.
Lafaysse, M., Morin, S., Coleou, C., Vernay, M., Serca, D., Besson, F., Willemet, J.-M., Giraud, G., Durand, Y., Oct. 2013. Towards a New Chain of Models for Avalanche Hazard Forecasting in French Mountain Ranges, Including Low Altitude Mountains. International Snow Science Workshop Grenoble – Chamonix Mont-Blanc - October 07–11, 2013, 162–165. http://arc.lib.montana.edu/snow-science/item/1741.
Larson, P.R., 1994. The Vascular Cambium: Development and Structure. Springer Science & Business Media google-Books-ID: 7mLwCAAAQBAJ.
Macciotta, R., Martin, C. D., Edwards, T., Cruden, D. M., Keegan, T., Jul. 2015. Quantifying weather conditions for rock fall hazard management. Georisk: Assess. Manage.Risk Eng. Syst. Geohazards 9 (3), 171–186. http://www.tandfonline.com/doi/full/10.1080/17499518.2015.1061673.
Mainieri, R., Corona, C., Chartoire, J., Eckert, N., Lopez-Saez, J., Stoffel, M., Bourrier, F., 2020. Dating of rockfall damage in trees yields insights into meteorological triggers of process activity in the French Alps. Earth Surf. Proc. Land. esp.4876.
Mainieri, R., Lopez-Saez, J., Corona, C., Stoffel, M., Bourrier, F., Eckert, N., 2019a. Assessment of the recurrence intervals of rockfall through dendrogeomorphology and counting scar approach: A comparative study in a mixed forest stand from the Vercors massif (French Alps). Geomorphology 340, 160–171 https://linkinghub.elsevier.com/retrieve/pii/S0169555X19302016.
Mainieri, R., Lopez-Saez, J., Corona, C., Stoffel, M., Mermin, E., Bourrier, F., Eckert, N., 2019b. L'inventaire forestier comme méthode de caractérisation spatiale de l'aléa chute de pierres. Schweizerische Zeitschrift fur Forstwesen 170 (2), 78–85 http://szf-jfs.org/doi/10.3188/szf.2019.0078.
Martin-Benito, D., Beeckman, H., Cañellas, I., 2013. Influence of drought on tree rings and tracheid features of Pinus nigra and Pinus sylvestris in a mesic Mediterranean forest. Eur. J. Forest Res. 132 (1), 33–45 http://link.springer.com/10.1007/s10342-012-0652-3.
Mateos, R.M., García-Moreno, I., Azañón, J.M., 2012. Freeze–thaw cycles and rainfall as triggering factors of mass movements in a warm Mediterranean region: the case of the Tramuntana Range (Majorca, Spain). Landslides 9 (3), 417–432 http://link.springer.com/10.1007/s10346-011-0290-8.
Matsuoka, N., 2019. A multi-method monitoring of timing, magnitude and origin of rockfall activity in the Japanese Alps. Geomorphology 336, 65–76 https://linkinghub.elsevier.com/retrieve/pii/S0169555X19301230.
Matsuoka, N., Sakai, H., 1999. Rockfall activity from an alpine cliff during thawing periods. Geomorphology 28 (3–4), 309–328 http://linkinghub.elsevier.com/retrieve/pii/S0169555X98001160.
Morel, P., Trappmann, D., Corona, C., Stoffel, M., 2015. Defining sample size and sampling strategy for dendrogeomorphic rockfall reconstructions. Geomorphology 236, 79–89 https://linkinghub.elsevier.com/retrieve/pii/S0169555X15001002.
Moya, J., Corominas, J., Pérez Arcas, J., Baeza, C., 2010. Tree-ring based assessment of rockfall frequency on talus slopes at Solà d'Andorra. Eastern Pyrenees. Geomorphol. 118 (3–4), 393–408 https://linkinghub.elsevier.com/retrieve/pii/S0169555X10000620.
Perret, S., Stoffel, M., Kienholz, H., 2006. Spatial and temporal rockfall activity in a forest stand in the Swiss Prealps—A dendrogeomorphological case study. Geomorphology 74 (1–4), 219–231 https://linkinghub.elsevier.com/retrieve/pii/S0169555X05002710.
Rabatel, A., Deline, P., Jaillet, S., Ravanel, L., 2008. Rock falls in high-alpine rock walls quantified by terrestrial lidar measurements: A case study in the Mont Blanc area: ROCK FALLS QUANTIFIED BY LIDAR. Geophys. Res. Lett. 35 (10) http://doi.wiley.com/10.1029/2008GL033424.
Sachs, T., Sep. 2005. Pattern Formation in Plant Tissues. Cambridge University Press, google-Books-ID: wZMdutJUelsC.
Sass, O., 2005. Temporal Variability of Rockfall in the Bavarian Alps, Germany. Arct. Antarct. Alp. Res. 37 (4), 564–573 https://www.jstor.org/stable/4095876.
Schneuwly, D., Stoffel, M., 2008a. Spatial analysis of rockfall activity, bounce heights and geomorphic changes over the last 50 years – A case study using dendrogeomorphology. Geomorphology 102 (3–4), 522–531 https://linkinghub.elsevier.com/retrieve/pii/S0169555X08002535.
Schneuwly, D.M., Stoffel, M., 2008b. Tree-ring based reconstruction of the seasonal timing, major events and origin of rockfall on a case-study slope in the Swiss Alps. In: Nat. Hazards Earth Syst. Sci..
Schneuwly, D.M., Stoffel, M., Bollschweiler, M., 2009. Formation and spread of callus tissue and tangential rows of resin ducts in Larix decidua and Picea abies following rockfall impacts. Tree Physiol. 29 (2), 281–289 https://academic.oup.com/treephys/article/29/2/281/1643370.
Selby, M.J., 1993. Hillslope Materials and Processes. second edition Edition. Oxford University Press, Oxford, New York.
Stoffel, M., 2008. Dating past geomorphic processes with tangential rows of traumatic resin ducts. URL http://boris.unibe.ch/85932/
Stoffel, M., Bollschweiler, M., 2008. Tree-ring analysis in natural hazards research – an overview. Nat. Hazards Earth Syst. Sci. 8 (2), 187–202 https://www.nat-hazards-earth-syst-sci.net/8/187/2008/.
Stoffel, M., Corona, C., 2014. Dendroecological Dating of Geomorphic Disturbance in Trees. Tree-Ring Res. 70 (1), 3–20 http://www.bioone.org/doi/abs/10.3959/1536-1098-70.1.3.
Stoffel, M., Liévre, I., Monbaron, M., Perret, S., 2005. Seasonal timing of rockfall activity on a forested slope at Täschgufer (Swiss Alps) – a dendrochronological approach. Zeitschrift für Geomorphologie.
Stoffel, M., Perret, S., 2006. Reconstructing past rockfall activity with tree rings: Some methodological considerations. Dendrochronologia 24 (1), 1–15 https://linkinghub.elsevier.com/retrieve/pii/S1125786506000178.
Stoffel, M., Schneuwly, D., Bollschweiler, M., Liévre, I., Delaloye, R., Myint, M., Monbaron, M., 2005. Analyzing rockfall activity (1600–2002) in a protection forest—a case study using dendrogeomorphology. Geomorphology 68 (3–4), 224–241 https://linkinghub.elsevier.com/retrieve/pii/S0169555X04003125.
Stoffel, M., Schneuwly, D.M., Bollschweiler, M., 2010. Assessing Rockfall Activity in a Mountain Forest – Implications for Hazard Assessment. In: Beniston, M., Stoffel, M., Bollschweiler, M., Butler, D.R., Luckman, B.H. (Eds.), Tree Rings and Natural

Hazards, Vol. 41. Springer, Netherlands, Dordrecht, pp. 139–155 http://link.springer.com/10.1007/978-90-481-8736-2_13.

Trappmann, D., Corona, C., Stoffel, M., 2013. Rolling stones and tree rings: A state of research on dendrogeomorphic reconstructions of rockfall. Prog. Phys. Geogr. 37 (5), 701–716 http://journals.sagepub.com/doi/10.1177/0309133313506451.

Trappmann, D., Stoffel, M., 2015. Visual dating of rockfall scars in Larix decidua trees. Geomorphology 245, 62–72 https://linkinghub.elsevier.com/retrieve/pii/S0169555X15002500.

Trappmann, D., Stoffel, M., Corona, C., 2014. Achieving a more realistic assessment of rockfall hazards by coupling three-dimensional process models and field-based tree-ring data: assessment of rockfalls by coupling rockfall models and tree-ring data. Earth Surf. Proc. Land. 39 (14), 1866–1875 http://doi.wiley.com/10.1002/esp.3580.

Vernay, M., Lafaysse, M., Hagenmuller, P., Nheili, R., Verfaillie, D., Morin, S., 2019. The S2M meteorological and snow cover reanalysis in the French mountainous areas (1958 - present). Medium: NetCDF 3 type: dataset. https://en.aeris-data.fr/metadata/?865730e8-edeb-4c6b-ae58-80f95166509b.

Weber, S., Beutel, J., Forno, R.D., Geiger, A., Gruber, S., Gsell, T., Hasler, A., Keller, M., Lim, R., Limpach, P., Meyer, M., Talzi, I., Thiele, L., Tschudin, C., Vieli, A., Vonder Mühll, D., Yücel, M., 2019. A decade of detailed observations (2008–2018) in steep bedrock permafrost at the Matterhorn Hörnligrat (Zermatt, CH). Earth Syst. Sci. Data 11 (3), 1203–1237 https://www.earth-syst-sci-data.net/11/1203/2019/.

Zielonka, A., Wronska-Walach, D., 2019. Can we distinguish meteorological conditions associated with rockfall activity using dendrochronological analysis? - An example from the Tatra Mountains (Southern Poland). Sci. Total Environ. 662, 422–433 http://www.sciencedirect.com/science/article/pii/S0048969719302980.